Effect of Iron and Silicon Content on the Hot Compressive Deformation Behavior of Dilute Al-Fe-Si Alloys

M. Shakiba, N. Parson, and X.-G. Chen

The hot deformation behavior of dilute Al-Fe-Si alloys (1xxx) containing various amounts of Fe (0.1 to 0.7 wt.%) and Si (0.1 to 0.25 wt.%) was studied by uniaxial compression tests conducted at various temperatures (350-550 °C) and strain rates (0.01-10 s^{-1}). The flow stress of the 1xxx alloys increased with increasing Fe and Si content. Increasing the Fe content from 0.1 to 0.7% raised the flow stress by 11-32% in Al-Fe-0.1Si alloys, whereas the flow stress increased 5-14% when the Si content increased from 0.1 to 0.25% in Al-0.1Fe-Si alloys. The influence of the temperature and the strain rate on the hot deformation behavior was analyzed using the Zener-Holloman parameter, and the effect of the chemical composition was considered in materials constants in the constitutive analysis. The proposed constitutive equations yielded an excellent prediction of the flow stress over wide ranges of temperature and strain rate with various Fe and Si contents. The microstructural analysis results revealed that the dynamic recovery (DRV) is the sole softening mechanism of the 1xxx alloys during hot deformation. Increasing the Fe and Si content retarded the DRV and resulted in a decrease in the subgrain size and mean misorientation angle of the boundaries.

1. Introduction

The 1xxx series aluminum alloys are primarily used for applications in which superior formability and excellent thermal and electrical conductivity are required. Typical applications include foil and strips for packaging, heat-exchanger tubing and fin stock, coaxial cable sheathing and electrical conductors (Ref 1, 2). These products are generally subjected to hot-forming processes such as extrusion and rolling. Therefore, the development of a method to analyze and predict their hot deformation behavior under various thermo-mechanical conditions is the primary goal.

The high-temperature flow behavior of various materials in hot-forming processes is very complex. The work hardening and dynamic softening are both significantly affected by many factors, such as the chemical composition, the forming temperature, the strain rate, and the strain (Ref 3, 4). The flow behavior of materials is very important for the design of hot-forming processes due to its substantial impact on the required deformation load as well as the kinetics of metallurgical transformations. Traditionally, the trial and error method has been employed to optimize the thermomechanical processes. To overcome the huge number of tests required to achieve a reliable conclusion in the trial and error practice, various modeling techniques have been developed that permit a significant reduction in the production cost.

The modeling of materials flow behavior is often conducted by proper constitutive equations, which correlates the dynamic material properties such as the flow stress to the process parameters such as the deformation temperature and strain rate (Ref 5-7). Normally, uniaxial hot compression tests are employed to provide the necessary data to extract the constitutive equations. Several analytical (Ref 8), phenomenological (Ref 9), and empirical (Ref 10) models have been proposed to describe the high temperature flow behavior for a wide range of metals and alloys. Johnson and Cook (Ref 11) proposed a phenomenological model to develop a cumulative-damage fracture model. Sellars et al. (Ref 12) proposed a hyperbolic sine constitutive law to describe the elevated temperature flow behavior of various materials. Sloof et al. (Ref 13) introduced a strain-dependent parameter into the hyperbolic sine constitutive equation to improve its accuracy. Lin et al. (Ref 14) proposed a revised hyperbolic sine constitutive equation to describe the flow behavior of 42CrMo steel by considering the compensation of the strain and strain rate. Ashtiani et al. (Ref 6) established strain-compensated constitutive equations to predict the flow behavior of commercially pure aluminum. Among various constitutive equations available, the hyperbolic sine constitutive equation, proposed by Sellars et al. (Ref 12), has proven to be applicable over a wide range of materials and alloys (Ref 5-7, 15, 16).

Commercial 1xxx aluminum alloys exhibit higher strength and work hardening than high purity aluminum. The main alloying additions, or controlled impurities, in these alloys are Fe and Si. Zhao et al. (Ref 17) reported that Fe and Si play a major role in the strength and work hardening of commercial 1xxx alloys and that the contribution from the other impurities is negligible. McQueen et al. (Ref 4, 18, 19) concluded that dynamic recrystallization (DRX) could not occur in

M. Shakiba and **X.-G. Chen**, Department of Applied Science, University of Québec at Chicoutimi, Saguenay, QC G7H 2B1, Canada; and **N. Parson**, Arvida Research and Development Centre, Rio Tino Alcan, Saguenay, QC G7S 4K8, Canada. Contact e-mail: mohammad.shakiba@uqac.ca.

commercially pure aluminum (1xxx alloys) and that dynamic recovery (DRV) was the sole restoration mechanism during hot deformation. Although a few researchers (Ref 4, 6, 19) have studied the hot deformation behavior of commercially pure aluminum, no systematic investigation of the influence of different Fe and Si contents on the hot deformation behavior of dilute Al-Fe-Si alloys is available in the literature.

In the present study, the hot deformation behavior of dilute Al-Fe-Si alloys with a systematic variation of the Fe and Si contents was investigated by hot compression tests conducted at various deformation temperatures and strain rates. The experimental stress-strain data were employed to drive constitutive equations correlating flow stress, deformation temperature, and strain rate considering the influence of the chemical composition. Moreover, the effects of the deformation conditions and the chemical composition on the microstructural evolution associated with the dynamic softening were investigated.

2. Experimental

To cover the range of Fe and Si of commercial interest in 1xxx alloys, seven dilute Al-Fe-Si alloys containing 0.1 to 0.7% Fe and 0.1 to 0.25% Si were investigated (all alloy compositions in this study are in wt.% unless otherwise indicated). The chemical compositions of the experimental alloys are presented in Table 1. They were prepared from commercially pure aluminum (99.7%), Al-20%Fe and Al-50%Si master alloys. For each composition, approximately 5 kg of material was melted in an electrical resistance furnace and then cast into a rectangular, permanent steel mold measuring $30 \times 40 \times 80$ mm^3. Prior to the cast, the melts were grain-refined by an addition of 0.015% Ti in the form of an Al-5Ti-1B master alloy. The cast ingots of these alloys were homogenized at 550 °C for 6 h, followed by water quenching at ambient temperature.

Cylindrical samples of 10 mm in diameter and 15 mm in height were machined from the homogenized ingots. The uniaxial hot compression tests were conducted using a Gleeble 3800 thermomechanical testing unit at strain rates of 0.01, 0.1, 1, and 10 s^{-1} and temperatures of 350, 400, 450, 500, and 550 °C. During the tests on the Gleeble 3800 unit, the specimens were heated at a rate of 2 °C/s and maintained for 120 s at the desired temperature to ensure a homogeneous temperature distribution. The specimens were deformed to a total true strain of 0.8 and then immediately water-quenched to retain the deformed microstructure.

The deformed samples were sectioned parallel to the compression axis along the centerline direction. Because conventional mechanical polishing can cause surface plastic

deformation on the relatively soft surfaces of commercially pure aluminum and introduces a large number of artifacts in the electron backscattered diffraction (EBSD) maps, an argon ion beam cross-section polisher (JEOL SM-09010) was employed in this study. All samples were polished in an Ar+ ion beam at 5 kV with a current of 80 mA for 8 h. The microstructural evolution of the compressed samples was investigated using the EBSD technique under a scanning electron microscope (SEM, JEOL JSM-6480LV). In the EBSD analysis, the boundaries of grains and subgrains are defined as low-angle boundaries, medium-angle boundaries, and high-angle boundaries with misorientation angles of 1-5°, 5-15°, and greater than 15°, respectively (Ref 20). The step size between the scanning points was set as 1.0 μm. The line intercept method was used to measure the subgrain size of the deformed samples. To ensure the statistical reliability, more than 100 subgrains were measured in each sample. For the quantitative measurement of the misorientation distribution of the boundaries, EBSD line scanning was performed with a step size of 0.2 μm.

3. Result and Discussion

3.1 Flow Stress Behavior

A series of true stress-true strain curves were obtained for all seven alloys at various deformation temperatures (350 to 550 °C) and strain rates (0.01 to 10 s^{-1}). Figure 1 and 2 display typical true stress-true strain curves for the Al-0.1Fe-0.1Si and Al-0.5Fe-0.1Si alloys as examples. At the beginning of deformation, the flow stress increased rapidly because of the dislocation multiplying and the high rate of work hardening (Ref 21, 22). Subsequently, the flow stress increased at a decreasing rate with an increase in the strain and then either remained fairly constant or, in certain cases with a high Zener-Holloman parameter (Z), continued to increase until the end of the deformation. The steady-state regime (after the strain of ~0.1) gives evidence of a constant dislocation density as a result of a balance of the work hardening and the dynamic softening. In the cases of high Z, the strain hardening without saturation is indicative of the work hardening being stronger than the dynamic softening during the deformation. In general, both flow behaviors are characteristic of high temperature deformation in which DRV is the dominant softening mechanism (Ref 18, 21, 23). The effects of the deformation temperature and strain rate on the flow stress behavior of these alloys were significant. The flow stress increased with decreasing deformation temperature and increasing strain rate, which is in good agreement with previously reported results (Ref 4, 6, 24). The highest value of the flow stress was obtained at a strain rate of 10 s^{-1} and a temperature of 350 °C for all of the alloys

Table 1 Chemical compositions of the experimental alloys (wt.%)

Alloys	Si	Fe	Cu	Mn	Cr	Ni	Ti	Zr	V
Al-0.1Fe-0.1Si	0.10	0.12	0.002	0.001	0.001	0.007	0.016	0.0015	0.012
Al-0.3Fe-0.1Si	0.10	0.28	0.003	0.002	0.001	0.007	0.017	0.0015	0.012
Al-0.5Fe-0.1Si	0.10	0.49	0.004	0.002	0.001	0.007	0.017	0.0014	0.012
Al-0.7Fe-0.1Si	0.11	0.68	0.006	0.003	0.001	0.007	0.018	0.0013	0.012
Al-0.1Fe-0.25Si	0.24	0.13	0.002	0.001	0.001	0.007	0.018	0.0014	0.012
Al-0.3Fe-0.25Si	0.24	0.30	0.001	0.002	0.001	0.007	0.017	0.0014	0.012
Al-0.5Fe-0.25Si	0.26	0.52	0.002	0.002	0.001	0.008	0.017	0.0015	0.012

investigated, whereas by decreasing the strain rate to 0.01 s^{-1} and increasing the temperature to 550 °C, the flow stress reached its minimum value.

Figure 3 and 4 demonstrate the influence of the Fe and Si levels on the flow stress at a strain of 0.8 for all of the alloys at two extremes of strain rates (0.01 and 10 s^{-1}), respectively. Increasing the Fe content increases the flow stress at all deformation conditions (Fig. 3). However, its effect was more significant when the Si level remained low (0.1%). For example, in the low Si series alloys (Al-Fe-0.1Si), at a given deformation condition (350 °C and 0.1 s^{-1}), increasing the iron content from 0.1 to 0.3% and 0.5% increased the flow stress from 34.9 to 38.3, and 40.2 MPa, respectively. In the high Si series alloys (Al-Fe-0.25Si), by raising the Fe content from 0.1 to 0.3, and 0.5, the flow stress increased from 39.5 to 42.1, and 42.8 MPa, respectively. Generally, in the case of the low Si alloys, raising the iron content from 0.1 to 0.5% increased the flow stress by 7 to 26% over the range of deformation conditions studied. However, by raising the iron content from 0.1 to 0.5 % in the high Si series alloys, the flow stress increased only 4 to 16%.

As seen in Fig. 4, the addition of Si can also increase the flow stress of dilute Al-Fe-Si alloys. Raising the silicon content from 0.1 to 0.25% in the Al-0.1Fe and Al-0.5Fe alloys increased the flow stress by 4 to 14% and 2 to 8%, respectively, over the range of deformation conditions applied. The results indicate that the influence of the Si content was more evident at a low Fe level. It appears that the impact of the individual alloy additions was more significant when the concentration of the other element was low.

3.2 Constitutive Analysis

Constitutive equations are widely used to model the hot deformation behavior of metals and alloys. At elevated temperature, the strain rate ($\dot{\varepsilon}$) is related to the temperature and flow stress, by the Arrhenius type equation (Ref 7, 13, 24, 25):

$$\dot{\varepsilon} = Af(\sigma)\exp\left(-\frac{Q}{RT}\right) \qquad \text{(Eq 1)}$$

where $\dot{\varepsilon}$ is the strain rate (s^{-1}), A is a constant, Q is the activation energy for hot deformation (kJ/mol), R is the universal gas constant (8.314 J/mol K), T is the absolute temperature (K) and $f(\sigma)$ is the stress function which can be expressed as (Ref 5, 15, 26-28):

$$f(\sigma) = \begin{cases} \sigma^{n_1} & \alpha\sigma \prec 0.8 \\ \exp(\beta\sigma) & \alpha\sigma \succ 1.2 \\ [\sinh(\alpha\sigma)]^n & \text{for all } \sigma \end{cases} \qquad \text{(Eq 2)}$$

where σ is the flow stress (MPa), n_1, β and n are material constant and $\alpha = \beta/n_1$ (Ref 26-28) is a stress multiplier. Generally, the power law equation break down at high stress values, and the exponential equation break down at low stress values. However, the hyperbolic sine law proposed by Sellars and McTegart (Ref 12), is suitable for constitutive analysis over a wide range of temperatures and strain rates (Ref 3, 7, 13, 24, 25). Furthermore, the effect of the temperature and the strain rate on the hot deformation behavior could be represented by the Zener-Holloman parameter (Z) in an exponential equation (Ref 6, 7, 21, 29):
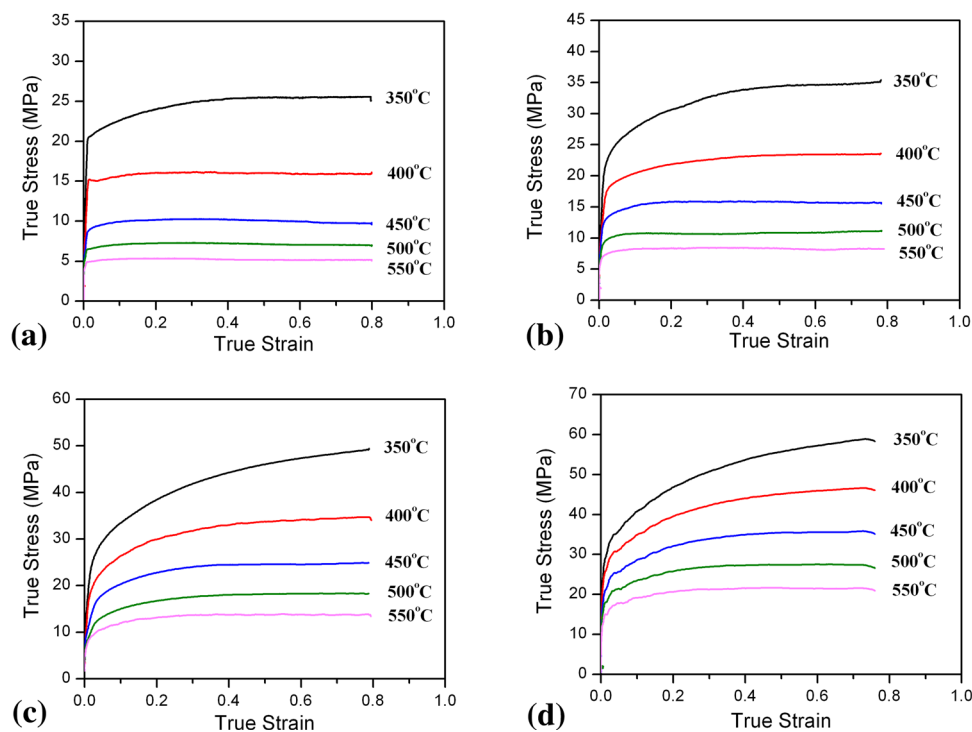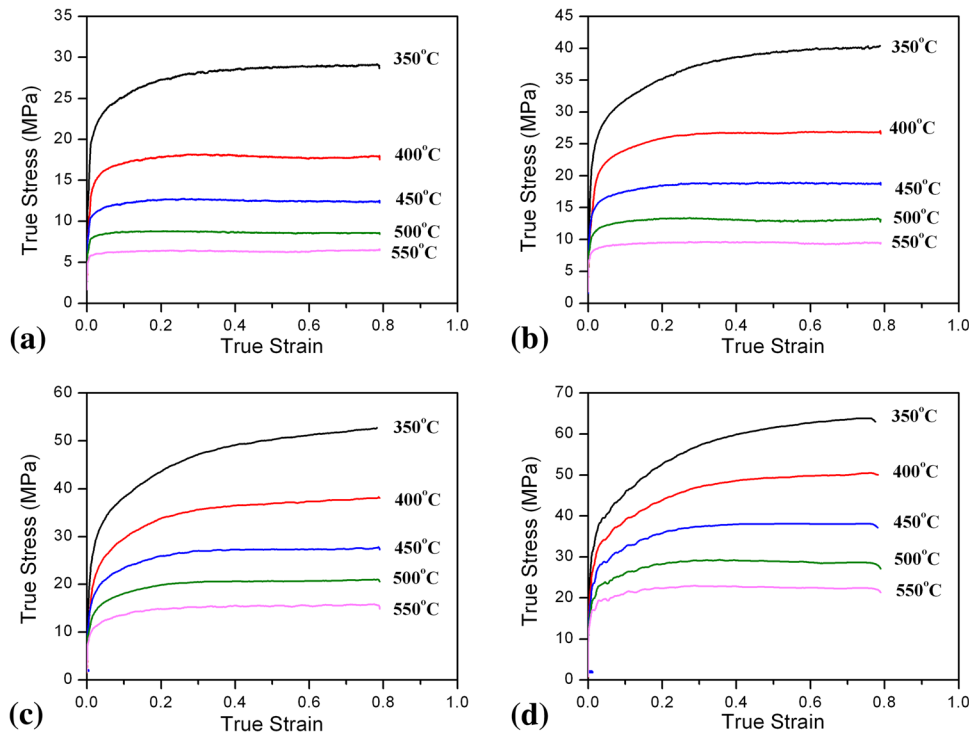

Fig. 1 True stress-true strain curves of the Al-0.1Fe-0.1Si alloy at various strain rates of (a) $\dot{\varepsilon} = 0.01$ s^{-1}, (b) $\dot{\varepsilon} = 0.1$ s^{-1}, (c) $\dot{\varepsilon} = 1$ s^{-1} and (d) $\dot{\varepsilon} = 10$ s^{-1}

Fig. 2 True stress-true strain curves of the Al-0.5Fe-0.1Si alloy at various strain rates of (a) $\dot{\varepsilon} = 0.01$ s^{-1}, (b) $\dot{\varepsilon} = 0.1$ s^{-1}, (c) $\dot{\varepsilon} = 1$ s^{-1} and (d) $\dot{\varepsilon} = 10$ s^{-1}
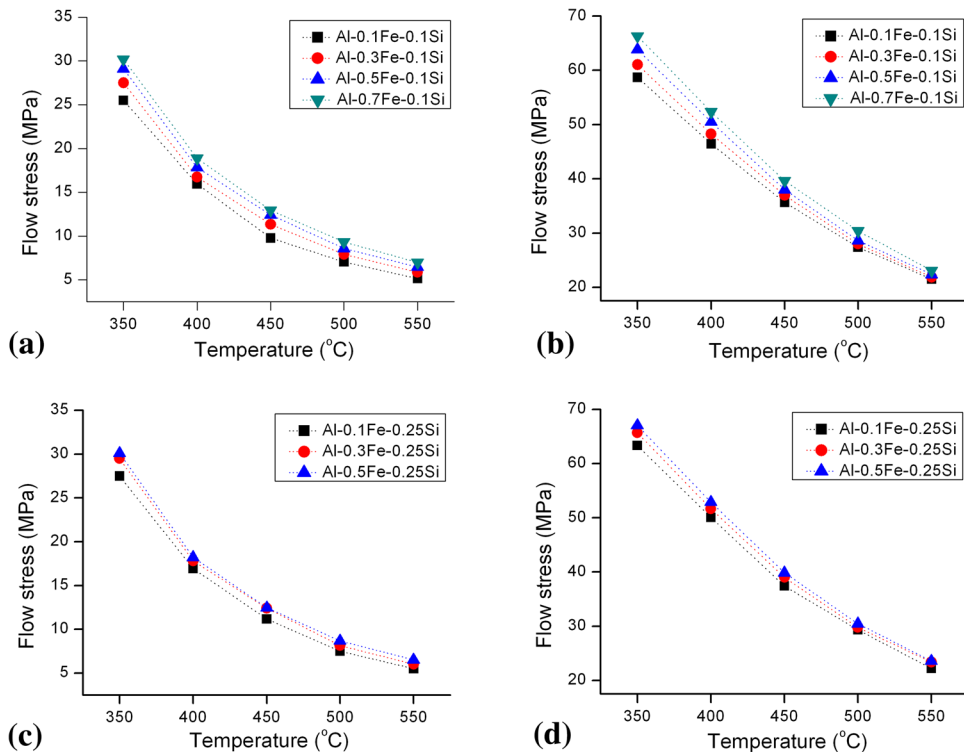

Fig. 3 Effect of iron on the flow stress at a strain of 0.8 and (a) Al-Fe-0.1Si $\dot{\varepsilon} = 0.01$ s^{-1}, (b) Al-Fe-0.1Si $\dot{\varepsilon} = 10$ s^{-1}, (c) Al-Fe-0.25Si $\dot{\varepsilon} = 0.01$ s^{-1} and (d) Al-Fe-0.25Si $\dot{\varepsilon} = 10$ s^{-1}
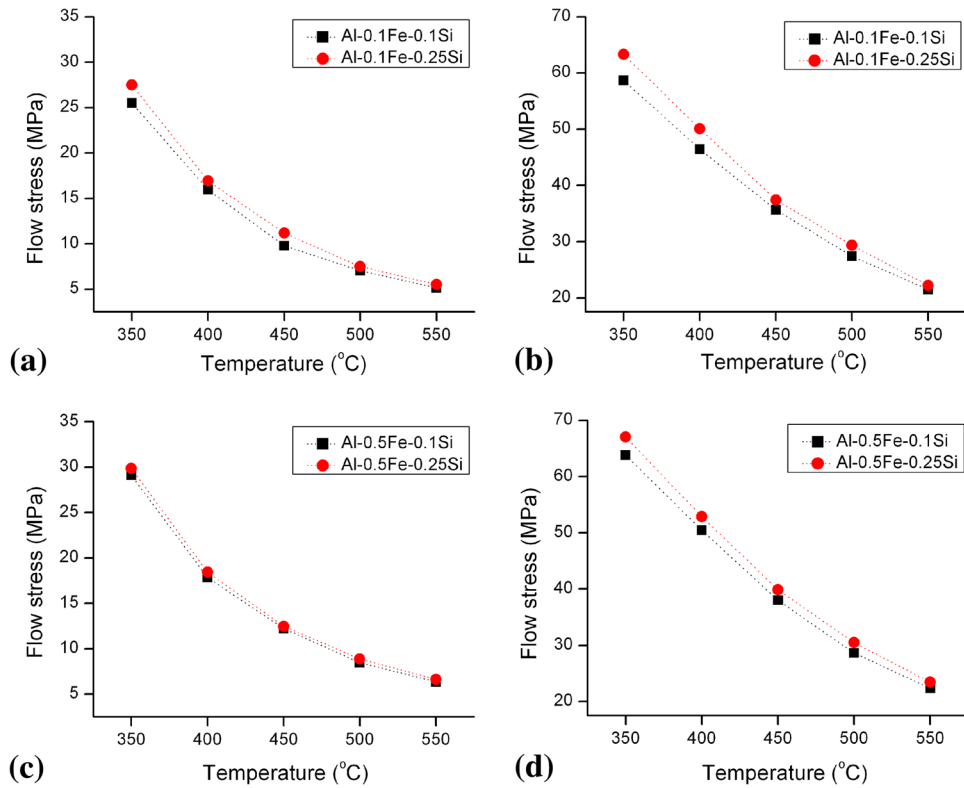
Fig. 4 Effect of silicon on the flow stress at a strain of 0.8 and (a) Al-0.1Fe-Si $\dot{\varepsilon} = 0.01$ s^{-1}, (b) Al-0.1Fe-Si $\dot{\varepsilon} = 10$ s^{-1}, (c) Al-0.5Fe-Si $\dot{\varepsilon} = 0.01$ s^{-1} and (d) Al-0.5Fe-Si $\dot{\varepsilon} = 10$ s^{-1}
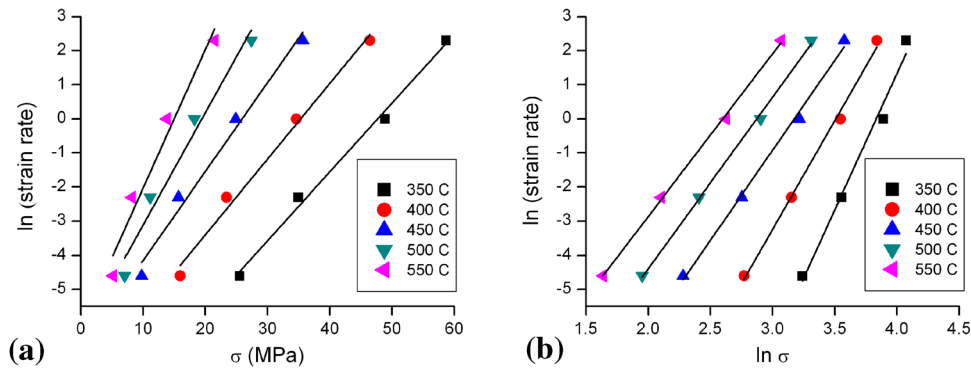

Fig. 5 plots of (a) $\ln \dot{\varepsilon} - \sigma$ and (b) $\ln \dot{\varepsilon} - \ln \sigma$ for the Al-0.1Fe-0.1Si alloy

$$Z = \dot{\varepsilon} \exp\left(\frac{Q}{RT}\right). \qquad \text{(Eq 3)}$$

Using the experimental results obtained from the hot compression tests at various temperatures and strain rates, the material constants and activation energy of the above mentioned equations could be determined for all alloys investigated. The following is the solution procedure for determining the materials constants and activation energy, using an Al-0.1Fe-0.1Si alloy as an example. In this study, the value of σ is taken from the value of the flow curves at a true stain of 0.8.

For the low ($\alpha\sigma < 0.8$) and the high ($\alpha\sigma > 1.2$) stress levels, substituting suitable function (the power law and exponential law of $f(\sigma)$) into Eq 1 leads to Eq 4 and 5, respectively:

$$\dot{\varepsilon} = A_1 \sigma^{n_1} \qquad \text{(Eq 4)}$$

$$\dot{\varepsilon} = A_2 \exp(\beta\sigma) \qquad \text{(Eq 5)}$$

where A_1 and A_2 are the material constants. Taking the natural logarithm of both sides of Eq 4 and 5 yields,

$$\ln(\sigma) = \frac{1}{n_1} \ln \dot{\varepsilon} - \frac{1}{n_1} \ln A_1 \qquad \text{(Eq 6)}$$

$$\sigma = \frac{1}{\beta}\ln\dot{\varepsilon} - \frac{1}{\beta}\ln A_2 \qquad \text{(Eq 7)}$$

Then, substituting the values of the flow stresses and corresponding strain rates into the Eq 6 and 7 gives the relationship between the flow stress and strain rate, as shown in Fig. 5. The value of β and n_1 could be obtained from the slope of the lines in the $\ln\dot{\varepsilon} - \sigma$ and $\ln\dot{\varepsilon} - \ln\sigma$ plots, respectively. The mean values of β and n_1 for the range of temperature studied were found to be 0.2841 and 5.8959, respectively. Consequently, the value of α was defined as $\alpha = \beta/n_1 = 0.048$ MPa^{-1}.

For wide range of stress level, Eq 1 could be represented as the hyperbolic sine law:

$$\dot{\varepsilon} = A[\sinh(\alpha\sigma)]^n \exp\left(-\frac{Q}{RT}\right) \qquad \text{(Eq 8)}$$

Differentiating Eq 8 results in:

$$Q = R\left[\frac{\partial \ln\dot{\varepsilon}}{\partial \ln[\sinh(\alpha\sigma)]}\right]_T \left[\frac{\partial \ln[\sinh(\alpha\sigma)]}{\partial(1/T)}\right]_{\dot{\varepsilon}} = RnS, \qquad \text{(Eq 9)}$$

where R is a universal gas constant, n is the mean slope of $\ln\dot{\varepsilon}$ versus $\partial\ln[\sinh(\alpha\sigma)]$ at various temperatures and S is the mean slope of the $\partial\ln[\sinh(\alpha\sigma)]$ versus $\partial(1000/T)$ at various strain rates. Figure 6 exhibits the relationship between $\ln\dot{\varepsilon} - \partial\ln[\sinh(\alpha\sigma)]$ and $\partial\ln[\sinh(\alpha\sigma)] - \partial(1000/T)$ for the Al-0.1Fe-0.1Si alloy. Therefore, the values of n, S and Q of the Al-0.1Fe-0.1Si alloy can be obtained from Fig. 6 and Eq 9.

Combining Eq 8 with Eq 3 results in:

$$Z = \dot{\varepsilon}\exp\left(\frac{Q}{RT}\right) = A[\sinh(\alpha\sigma)]^n. \qquad \text{(Eq 10)}$$

Taking the natural logarithm of both sides of Eq 10 results in:

$$\ln Z = \ln A + n\ln[\sinh(\alpha\sigma)]. \qquad \text{(Eq 11)}$$

The linear correlation between $\ln Z$ and $\ln[\sinh(\alpha\sigma)]$ are shown in Fig. 7. The value of $\ln A$ is the intercept of the plot of $\ln Z$ versus $\ln[\sinh(\alpha\sigma)]$.

In a similar way, the values of the materials constants, α, n, and A, as well as the activation energy, Q, can be computed for all of the other alloys. Table 2 presents the values of the materials constants and activation energies corresponding to all of the alloys investigated. As can be seen, the value of α

decreases as the values of n, A, and Q increase with increasing Fe or Si contents. The calculated values of the activation energies of 1xxx alloys lie between 167 and 182 kJ/mol in this study, values which are in general agreement with those reported previously for commercially pure aluminum (Ref 3, 4, 19, 21, 30, 31).

3.3 Effect of the Chemical Composition

So far, the constitutive equations have been employed to study the influences of deformation conditions such as the temperature and strain rate on the flow stress of individual alloys with a specific chemical composition. As can be seen, the effect of the chemical composition is not considered in Eq 1 and 3. In this section, the effects of the chemical composition on the materials constants and activation energy in the constitutive equations were also considered. Fulfilling this goal, the values of the materials constants and activation energy (α, n, $\ln A$ and Q) obtained from the constitutive equations are considered as a function of the Fe content. Figure 8 illustrates the variation in the materials constants and activation energy with differing Fe contents for both the low- and high-Si series alloys. A second-order polynomial function, as shown in Eq 12, was found to represent the influence of the Fe content with very good correlation and generalization (Fig. 8). The
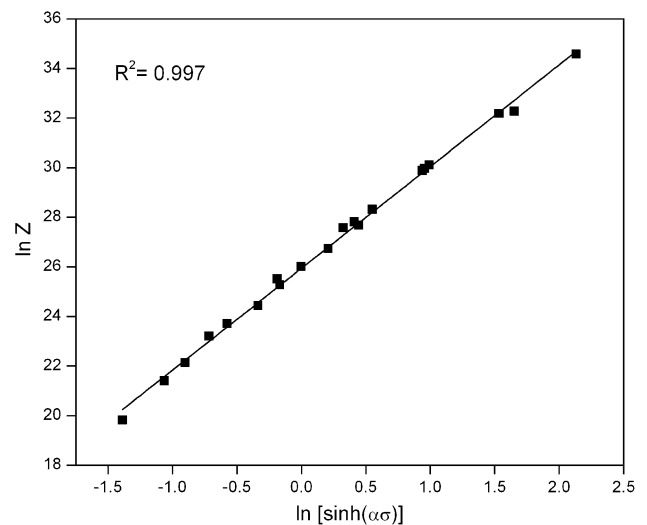
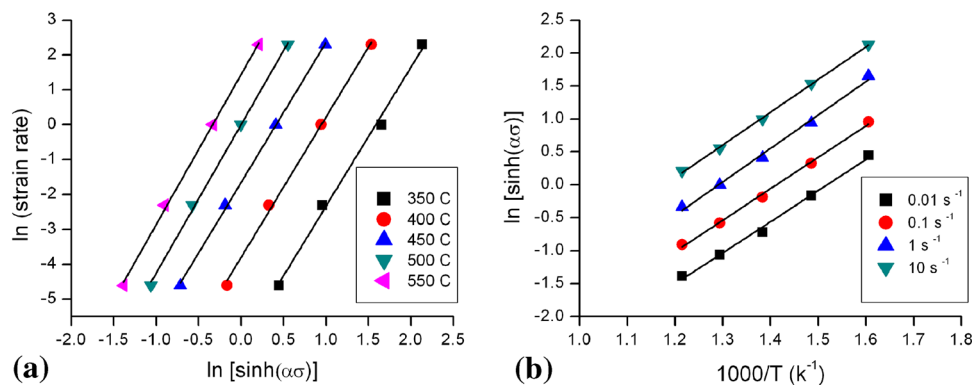**Fig. 7** Plot of $\ln Z$ vs. $\ln[\sinh(\alpha\sigma)]$ for the Al-0.1Fe-0.1Si alloy

Fig. 6 Plots of (a) $\ln\dot{\varepsilon}$ vs. $\ln[\sinh(\alpha\sigma)]$ and (b) $\ln[\sinh(\alpha\sigma)]$ vs. $(1000/T)$ for the Al-0.1Fe-0.1Si alloy

Table 2 Values of materials constants and activation energies of all experimental alloys

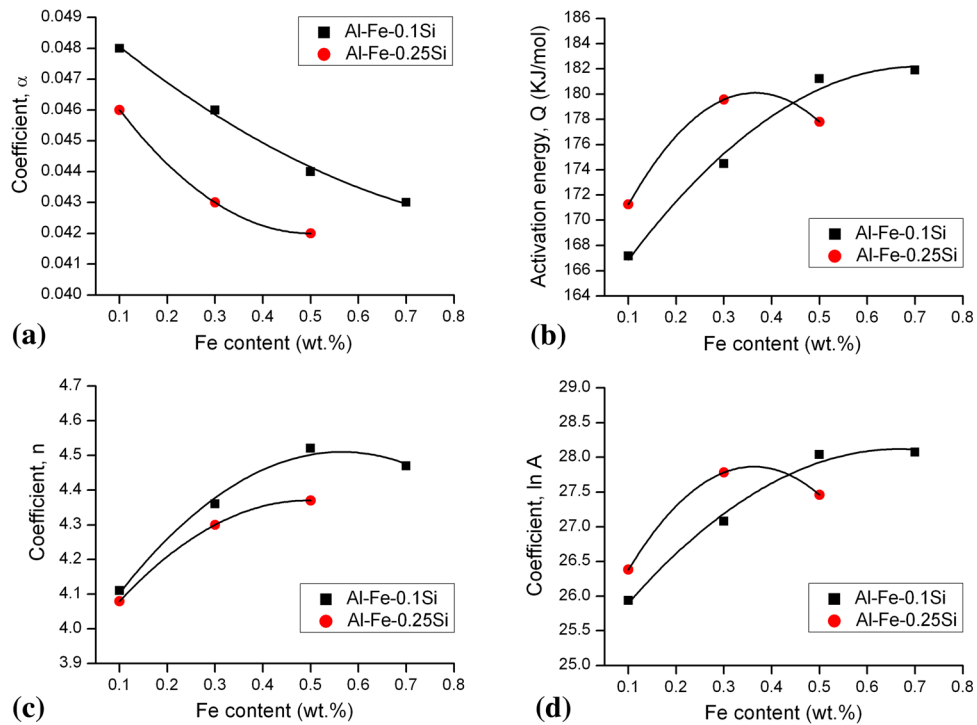| Alloys	α, MP^{-1}	n	A, s^{-1}	Q, kJ/mol
Al-0.1Fe-0.1Si	0.048	4.11	1.84E+11	167.2
Al-0.3Fe-0.1Si	0.046	4.36	5.75E+11	174.5
Al-0.5Fe-0.1Si	0.044	4.52	1.50E+12	181.2
Al-0.7Fe-0.1Si	0.043	4.48	1.55E+12	181.9
Al-0.1Fe-0.25Si	0.046	4.08	2.87E+11	171.3
Al-0.3Fe-0.25Si	0.043	4.30	1.16E+12	179.6
Al-0.5Fe-0.25Si	0.042	4.35	8.42E+11	177.8

Fig. 8 Relationship between (a) α (b) Q, (c) n and (d) ln A and the Fe level by a polynomial fit for both Al-Fe-0.1Si and Al-Fe-0.25Si alloys

Table 3 Coefficients of the polynomial fit of α, Q, n and ln A for the Al-Fe-0.1Si alloy

α		Q		n		ln A	
B_0	0.0493	C_0	161.44	D_0	3.9108	E_0	25.049
B_1	−0.0135	C_1	58.565	D_1	2.12	E_1	9.2095
B_2	0.0063	C_2	−41.313	D_2	−1.875	E_2	−6.9063

Table 4 Coefficients of the polynomial fit of α, Q, n and ln A for the Al-Fe-0.25Si alloy

α		Q		n		ln A	
B_0	0.0483	C_0	163.34	D_0	3.9063	E_0	25.04
B_1	−0.025	C_1	91.85	D_1	1.95	E_1	15.595
B_2	0.025	C_2	−125.87	D_2	−2.125	E_2	−21.512

coefficients of the polynomial fit are provided in Tables 3 and 4 for the alloys containing 0.1 and 0.25 Si, respectively.

$$\alpha = B_0 + B_1 Fe + B_2 Fe^2$$
$$Q = C_0 + C_1 Fe + C_2 Fe^2$$
$$n = D_0 + D_1 Fe + D_2 Fe^2 \qquad \text{(Eq 12)}$$
$$LnA = E_0 + E_1 Fe + E_2 Fe^2$$

where Fe is the Fe content in wt.%.

Figure 8 demonstrates that the polynomial function provides a good description of the relationship between the materials constants and the Fe level in 1xxx alloys. The value of α decreases with increasing Fe content, whereas the values of n and A increase with increasing Fe contents for both the low and high Si alloys. Moreover, the activation energy for hot deformation, Q, is an important indicator of the degree of difficulty of plastic deformation. The change in the hot deformation activation energy as a function of the Fe content for both the low and high Si series are shown in Fig. 8(b). The Q values gradually increase with increasing Fe content in all of the alloys except for Al-0.5Fe-0.25Si. It is worth noting that the effect of the Fe content on the activation energy is more significant at low Fe levels. By increasing the Fe content from 0.1 to 0.5% in the low Si series alloys, the Q value increases from 167.2 to 181.2 kJ/mol, whereas its value only slightly increases from 181.2 to 181.9 kJ/mol as the Fe content increases from 0.5 to 0.7%. On the other hand, the value of the activation energy even slightly decreases from 179.6 to 177.8 kJ/mol in the high Si series alloys as the Fe content increases from 0.3 to 0.5%.

From Eq 10, the flow stress, σ, can be expressed as a function of the Zener-Hollomon parameter as follows:

$$\sigma = \frac{1}{\alpha} \ln \left\{ \left(\frac{Z}{A} \right)^{1/n} + \left[\left(\frac{Z}{A} \right)^{2/n} + 1 \right]^{1/2} \right\}. \qquad \text{(Eq 13)}$$

After the relationship between the materials constants and the Fe content are well established, the flow stress of the 1xxx alloys with various compositions (Fe level) at any given deformation condition can be predicted by employing Eq 13.

To verify the constitutive equations developed for dilute Al-Fe-Si alloys, the predicted flow stress values were plotted against the experimental flow stress measurements (Fig. 9). The correlation coefficients between the experimental and predicted results were greater than 99% for all of the alloys investigated. It can be seen that the proposed models could accurately predict the flow stress of 1xxx alloys through the entire range of Fe contents, temperatures, and strain rates, which means that they can be used for numerical simulation of the hot deformation process and in choosing the proper deformation parameters in commercial practice.

3.4 Microstructural Evolution During Hot Deformation

Figure 10 illustrates optical micrographs of Al-0.1Fe-0.1Si and Al-0.5Fe-0.25Si alloys after homogenization. Because the solid solubility of iron in aluminum is very low (i.e., max. 0.05% at 650 °C), most of the iron combines with both aluminum and silicon to form secondary Fe-rich intermetallic phases (Ref 32, 33). These Fe-rich intermetallic particles are distributed predominantly in the dendrite cell boundaries. In the homogenized microstructure, the dominant constituent phase was Al_3Fe in the low Si series alloys, whereas in the high Si
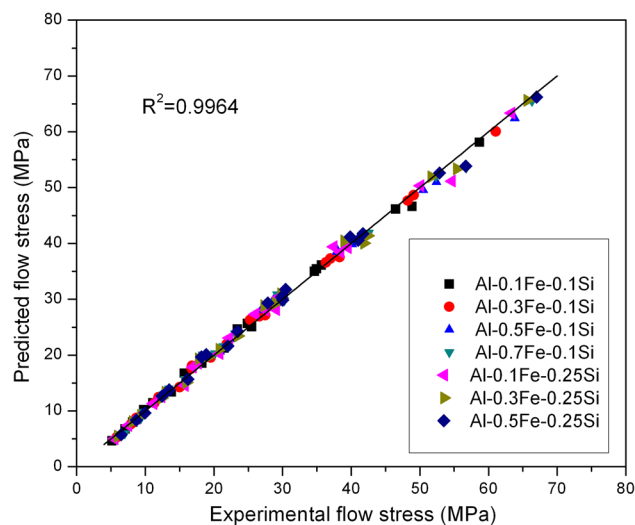

Fig. 9 Correlation between the experimental and predicted flow stress of 1xxx alloys

series alloys, the major phase was α-AlFeSi. With increasing Fe content, the number of Fe-rich intermetallic particles increases. Increasing the Si content increases the amounts of the constituent particles and solute atoms simultaneously. A detailed description of the Fe-rich intermetallic phases in dilute Al-Fe-Si alloys and the effects of homogenization were reported in our previous study (Ref 34).

To study the influence of the deformation conditions on the microstructural evolution of Al-Fe-Si alloys, the Al-0.1Fe-0.1Si composition was selected to be analyzed by EBSD, and the effect of the deformation conditions on the misorientation angle of the boundaries and the subgrain size were quantitatively evaluated. Figure 11 shows orientation imaging maps of the deformed microstructure under various deformation conditions for the Al-0.1Fe-0.1Si alloy after compression to a strain of 0.8. In hot-worked aluminum alloys, the original grain boundaries are generally characterized by high-angle boundaries ($>15°$), whereas low-angle boundaries (1-5°) and medium-angle boundaries (5-15°) form subgrain structures (Ref 22).

During hot deformation, the original grains were elongated perpendicular to the compression direction. The deformation performed at a high Z condition (400 °C and 10 s^{-1}) resulted in a high density of low-angle boundaries and consequently a great number of small subgrains (Fig. 11a). Irregular deformation bands were observed inside the original grains (see arrows in Fig. 11a) due to the deformation occurring on a different slip system (Ref 22). When the strain rate was reduced to 0.01 s^{-1} at a temperature of 400 °C, the deformation bands became less visible, and larger subgrains were formed with neatly arranged boundaries (Fig. 11b), thereby indicating an increased level of DRV due to the greater time for dislocation polygonization (Ref 22). Furthermore, when the temperature increased to 500 °C at a strain rate of 0.01 s^{-1}, the substructure was further recovered, which involved the rearrangement and annihilation of dislocations, resulting in the presence of coarsened subgrains with higher-angle boundaries (Fig. 11c). The increased polygonization consisted of an enlargement of the subgrains and the rearrangement of the subboundary dislocations into neater networks (Ref 19).

Table 5 shows the variation in the mean misorientation angle and the subgrain sizes with the deformation conditions in
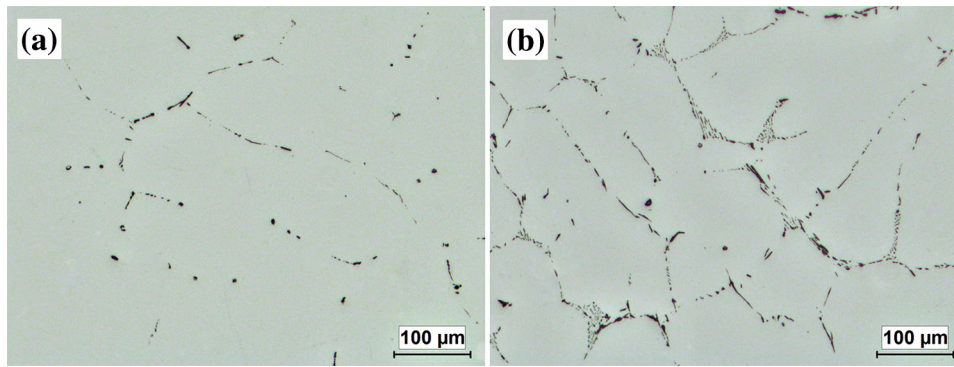
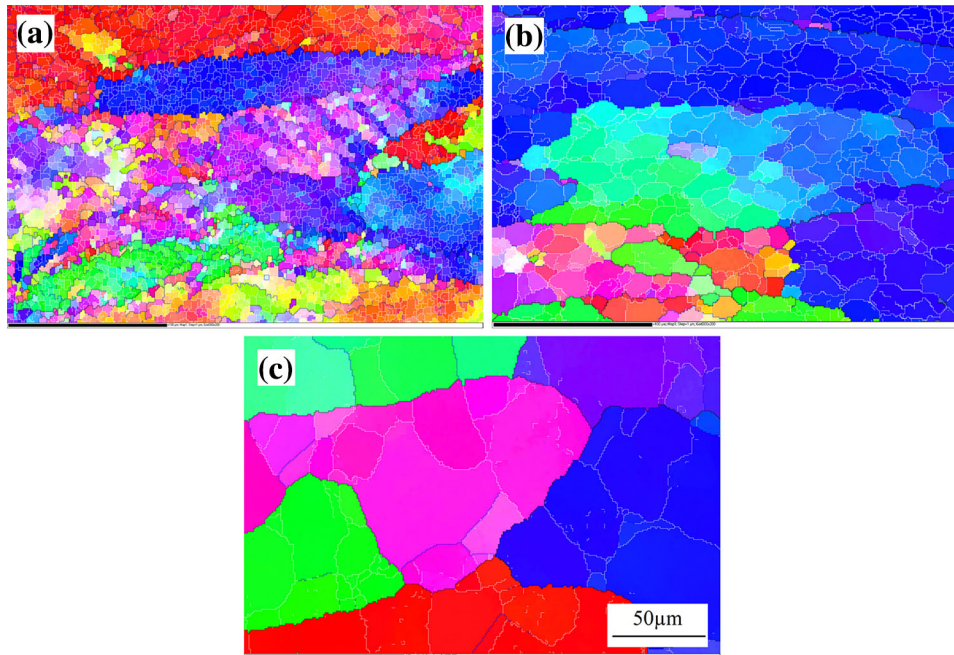**Fig. 10** As-homogenized microstructures of (a) Al-0.1Fe-0.1Si and (b) Al-0.5Fe-0.1Si

Fig. 11 Orientation imaging maps of the Al-0.1Fe-0.1Si alloy under various deformation conditions: (a) 10 s^{-1}, 400 °C, (b) 0.01 s^{-1}, 400 °C and (c) 0.01 s^{-1}, 500 °C. White lines are 1-5°, blue lines are 5-15° and black lines are >15°

Table 5 Evolution of the mean misorientation angle and the subgrain size under various deformation conditions in the Al-0.1Fe-0.1Si alloy

Deformation condition	Mean misorientation angle, °	Subgrain size, μm
400 °C/10 s^{-1}	7.42	3.58
400 °C/0.01 s^{-1}	9.27	7.29
500 °C/0.01 s^{-1}	13.27	16.52

the Al-0.1Fe-0.1Si alloy. As the temperature increased and the strain rate decreased, both the mean misorientation angle of the boundaries and the subgrain size increased. This suggests a higher rate of DRV with increasing temperature and decreasing strain rate (Ref 21, 22), which is consistent with the microstructural observations shown in Fig. 11. The DRV is a thermally activated process, of which the level is improved as the temperature increases (Ref 22). When the strain rate decreases, the increased level of DRV is attributed to the increased time for subgrain coalescence (Ref 21, 22).

To understand the effect of the Fe and Si content on the microstructural evolution of 1xxx alloys, a fixed deformation condition (500 °C and 0.01 s^{-1}) was selected to compare different alloys. Figure 12 illustrates the orientation imaging maps of the deformed samples with various Fe and Si contents. The impact of Fe on the subgrain structure can be seen from Fig. 11(c) and 12(a) and (b) as the Fe content increases from 0.1 via 0.3 to 0.5%. Generally, those samples displayed a similar deformed microstructure, in which solely DRV occurred during hot deformation. However, the levels of the DRV of those samples varied with the Fe contents, as also shown in Fig. 13. At a given Si content, both the mean misorientation angle of the boundaries and the subgrain size were continuously decreased with increasing Fe contents. For example, the Al-0.7Fe-0.1Si alloy displays the smallest mean misorientation angle and subgrain size among the four low Si alloys,
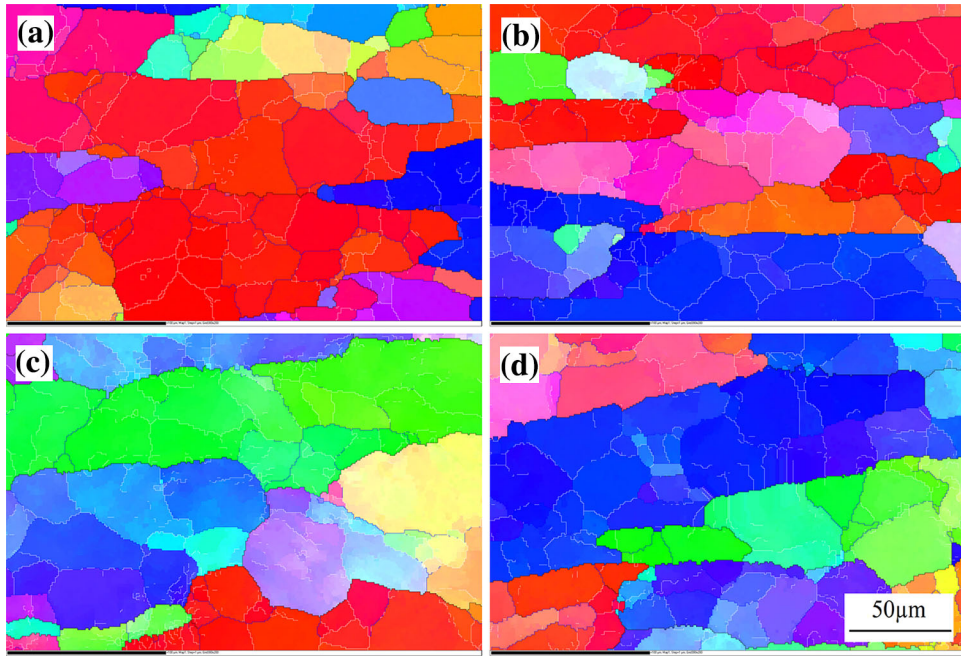
Fig. 12 Orientation imaging maps of the (a) Al-0.3Fe-0.1Si, (b) Al-0.5Fe-0.1Si, (c) Al-0.1Fe-0.25Si and (d) Al-0.5Fe-0.25Si alloys deformed at 500 °C and 0.01 s^{-1}
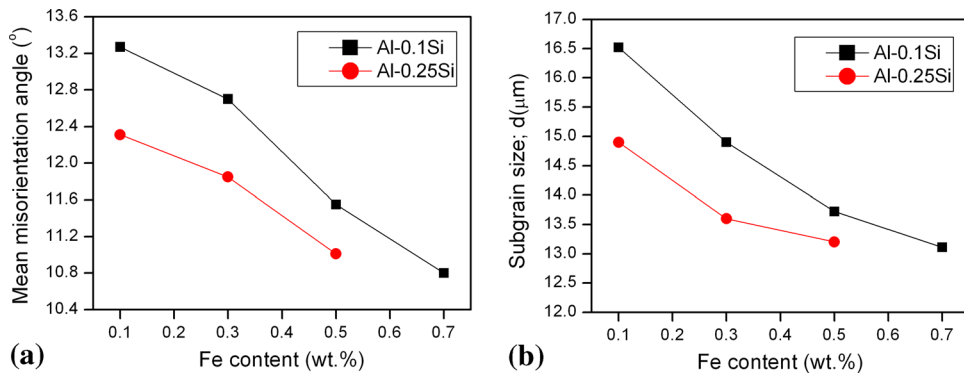

Fig. 13 Effect of the Fe and Si content on (a) the mean misorientation angle and (b) the subgrain size of 1xxx alloys deformed at 500 °C and 0.01 s^{-1}
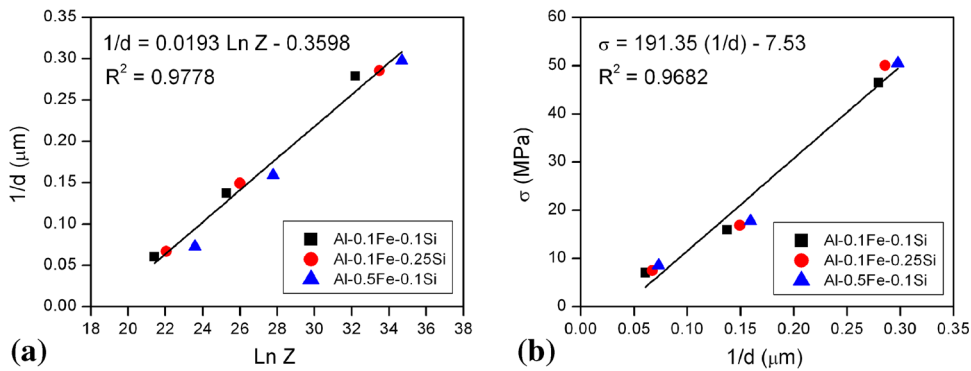

Fig. 14 Relationship between (a) the reciprocal subgrain diameter (d^{-1}) and the logarithm of the Zener-Hollomon parameter (Z) and (b) the steady-state flow stress (σ) and the reciprocal subgrain diameter (d^{-1})

indicating a slowing of the DRV with increased Fe content. On the other hand, when comparing Fig. 11(c) with 12(c) and (b) with (d), it is found that the high-Si alloys exhibited finer subgrain structures relative to the low-Si alloys. At the same Fe content, the higher the Si level, the lower the mean misorientation angle and the smaller the subgrain size were (Fig. 13). These results indicate a decreased level of DRV as the Si content increases. To find a quantitative relationship between the average subgrain diameter and the deformation conditions, three alloys (Al-0.1Fe-0.1Si, Al-0.1Fe-0.25Si and Al-0.5Fe-0.1Si) were selected for analysis. Figure 14(a) shows the relationship between the deformation conditions (Z) and the subgrain diameter (d). It is apparent that the subgrain size became smaller as the Zener-Hollomon parameter increased, and a good linear fit between the reciprocal subgrain diameter and the logarithm of the Zener-Hollomon parameter is found, as expressed in Eq 14:

$$d^{-1} = 0.0193 \ln Z - 0.3598. \qquad \text{(Eq 14)}$$

Figure 14(b) illustrates the relationship between the steady-state flow stress and the subgrain diameter. It is evident that the flow stress increases with decreasing subgrain diameter, and a linear function between the steady-state flow stress and the reciprocal subgrain diameter, based on the equation proposed by McQueen et al. (Ref 35) and Jonas et al. (Ref 36), is established (Eq 15):

$$\sigma_s = 191.35 d^{-1} - 7.53. \qquad \text{(Eq 15)}$$

The deformation conditions (Z), such as the temperature and strain rate define the steady-state subgrain size, which in turn determines the flow stress. As the temperature decreased and the strain rate increased, a high flow stress was induced as a result of the fine subgrain size generated during hot deformation. It should be mentioned that this relation could not be used at very high temperatures where the subgrain size becomes very large (>25 μm).

Based on the microstructural observations in Fig. 11 and 12, it is clear that DRV is the sole softening mechanism that operates during hot deformation of the dilute Al-Fe-Si alloys. The subgrain structures in these figures were the result of the mutual annihilation of many dislocations and the rearrangement of the remaining dislocation into regular low/medium-angle boundaries. This phenomenon is commonly observed during deformation in metals and alloys with high stacking fault energies (Ref 4, 18, 21). The relatively high rate of DRV significantly offsets the work-hardening effect and reduces the driving force for DRX (Ref 21, 22). It is evident that the level of DRV increases when the deformation temperature increases and the strain rate decreases, which is associated with an increase in the mean misorientation angle of the boundaries and the subgrain size (Table 5). Furthermore, the addition of Fe and Si enhances the strain hardening and impedes DRV during hot deformation, leading to a finer subgrain structure (Fig. 12 and 13). In the case of Fe addition, Fe-rich intermetallic particles greater than several μm in length cannot be sheared or bypassed by the moved dislocations (Ref 21). The plastic deformation is performed by the flow of the aluminum matrix around them, which is associated with a local lattice rotation in the vicinity of the intermetallic particles (Ref 22). This results in an increased deformation resistance and the formation of smaller subgrains near the intermetallic particles (Ref 21, 22). With a higher Fe content, the increased amount of Fe-rich intermetallic particles acts as a stronger barrier to deformation and thus results in a further increase in the flow stress and a decrease in the overall subgrain size. On the other hand, Si addition increases both the amounts in Si solute atoms and intermetallic particles. The deformation resistance is increased due to the solute-drag effect and the enhanced barrier to plastic flow (Ref 21, 22, 37). Therefore, at a given Fe addition, the alloy with a higher Si content demonstrates an increase in the flow stress and a decrease in the level of DRV.

The use of extruded 1xxx alloys is commercially important for the production of thin-walled tubing for refrigeration, heat transfer and conductor applications. Given the perceived simplicity of this alloy family, there is a surprisingly wide range of alloys in commercial use just for extruded applications, including AA1050, AA1060, AA1235, AA1100, and AA1350, with many compositional variants within the registered AA specifications. Extrudability is a term used to capture the ability to process an alloy at high speed into thin-walled shapes; for 1xxx alloys, for which the extrusion ratios are high even with multistranding, this is primarily controlled by the flow stress. In general, this alloy family is considered to have good extrudability due to its dilute nature and high melting point. However, the current work has indicated that small changes in the iron and silicon content can have a significant impact on the flow stress and thus on the extrusion productivity and cost, which is an important aspect that should be considered for alloy selection and design.

4. Conclusions

In the present study, the hot deformation behavior of dilute Al-Fe-Si alloys with a systematic variation in the Fe and Si contents was studied. From the results obtained, the following conclusions can be drawn.

(1) Increasing the iron content increased the high temperature flow stress for all of the alloys studied. In the case of low Si (0.10%) alloys, increasing the iron level from 0.1 to 0.7% produced 11 to 32% increase in the flow stress over the range of deformation conditions investigated. However, for high Si (0.25%) alloys, by increasing the iron level from 0.1 to 0.5%, the flow stress increased only 4 to 16%.

(2) The addition of silicon also increased the high temperature flow stress. Increasing the silicon level from 0.1 to 0.25 % in the Al-0.1Fe and Al-0.5Fe alloys increased the flow stress by 4-14% and 2-8%, respectively, over the range of deformation conditions investigated.

(3) The materials constants and activation energies for hot deformation as a function of the Fe content were determined from the experimental compression data obtained. The applied constitutive equations yielded an excellent predication of the flow stress over wide temperature and strain-rate ranges of 1xxx alloys with various Fe and Si contents.

(4) The activation energy for hot deformation gradually increased with increasing Fe and Si contents. Increasing the Fe content from 0.1 to 0.7% in low Si alloys increased the activation energy from 167.2 to 181.9 kJ/mol, whereas increasing the Si level from 0.1 to 0.25%

in the Al-0.1Fe-Si alloy raised the activation energy from 167.2 to 171.2 kJ/mol.

(5) DRV is the sole softening mechanism operating during the hot deformation of dilute Al-Fe-Si alloys. The rate of the DRV increased with increasing deformation temperature and decreasing strain rate. Increasing the Fe and Si contents promoted the retardation of the DRV due to the increased amounts of intermetallic particles and Si solute atoms in the aluminum matrix.

(6) The impact of small changes in the Fe and Si contents on the flow stress and resulting extrudability of 1xxx alloys is significant, and this fact should be considered in alloy selection and design for extruded applications.

References

1. J.R. Davis, *Aluminum and Aluminum Alloys*, Materials Park, OH, ASM International, 1993, p 59–87

2. J.G. Kaufman, *Introduction to Aluminum Alloys and Tempers*, Materials Park, OH, ASM International, 2000, p 87–118

3. H.J. McQueen and N.D. Ryan, Constitutive Analysis in Hot Working, *Mater. Sci. Eng. A*, 2002, **322**, p 43–63

4. H.J. McQueen, E. Evangelista, N. Jin, and M.E. Kassner, Energy Dissipation Efficiency in Aluminum Dependent on monotonic Flow Curves and Dynamic Recovery, *Metall. Mater. Trans. A*, 1995, **26**, p 1757–1766

5. H. Mirzadeh, A. Najafizadeh, and M. Moazeny, Flow Curve Analysis of 17-4PH Stainless Steel Under Hot Compression Test, *Metall. Mater. Trans. A*, 2009, **40**, p 2950–2958

6. H.R. Rezaei Ashtiani, M.H. Parsa, and H. Bisadi, Constitutive Equations for Elevated Temperature Flow Behavior of Commercial Purity Aluminum, *Mater. Sci. Eng. A*, 2012, **545**, p 61–67

7. Y.C. Lin, Y.-C. Xia, X.-M. Chen, and M.-S. Chen, Constitutive Descriptions for Hot Compressed 2124-T851 Aluminum Alloy over a Wide Range of Temperature and Strain Rate, *Comput. Mater. Sci.*, 2010, **50**, p 227–233

8. J. Luo, M. Li, X. Li, and Y. Shi, Constitutive Model for High Temperature Deformation of Titanium Alloys Using Internal State Variables, *Mech. Mater.*, 2010, **42**, p 157–165

9. Y.C. Lin, Q.-F. Li, Y.-C. Xia, and L.-T. Li, A Phenomenological Constitutive Model for High Temperature Flow Stress Prediction of Al-Cu-Mg Alloy, *Mater. Sci. Eng. A*, 2012, **534**, p 654–662

10. S.B. Davenport, N.J. Silk, C.N. Sparks, and C.M. Sellars, Development of Constitutive Equations for Modelling of Hot Rolling, *Mater. Sci. Technol.*, 2000, **16**, p 539–546

11. G.R. Johnson and W.H. Cook, Fracture Characteristics of Three Metals Subjected to Various Strains, Strain Rates, Temperatures and Pressures, *Eng. Fract. Mech.*, 1985, **21**, p 31–48

12. C.M. Sellars and W.J. McTegart, La relation entre la résistance et la structure dans la déformation à chaud, *Mem. Sci. Rev. Met.*, 1966, **63**, p 731–746 ((in French))

13. F.A. Slooff, J. Zhou, J. Duszczyk, and L. Katgerman, Constitutive Analysis of Wrought Magnesium Alloy Mg-Al4-Zn1, *Scr. Mater.*, 2007, **57**, p 759–762

14. Y.-C. Lin, M.-S. Chen, and J. Zhong, Constitutive Modeling for Elevated Temperature Flow Behavior of 42CrMo Steel, *Comput. Mater. Sci.*, 2008, **42**, p 470–477

15. Y.-C. Lin, M.-S. Chen, and J. Zhang, Modeling of Flow Stress of 42CrMo Steel Under Hot Compression, *Mater. Sci. Eng. A*, 2009, **499**, p 88–92

16. C. Shi and X.-G. Chen, Effect of Zr Addition on Hot Deformation Behavior and Microstructural Evolution of AA7150 Aluminum Alloy, *Mater. Sci. Eng. A*, 2014, **596**, p 183–193

17. Q. Zhao, M. Slagsvold, and B. Holmedal, Comparison of the Influence of Si and Fe in 99.999% Purity Aluminum and in Commercial-Purity Aluminum, *Scr. Mater.*, 2012, **67**, p 217–220

18. H.J. McQueen and W. Blum, Dynamic Recovery: Sufficient Mechanism in the Hot Deformation of Al, *Mater. Sci. Eng. A*, 2000, **290**, p 95–107

19. H. McQueen and J. Hockett, Microstructures of Aluminum Compressed at Various Rates and Temperatures, *Metall. Trans.*, 1970, **1**, p 2997–3004

20. F.J. Humphreys, Review Grain and Subgrain Characterisation by Electron Backscatter Diffraction, *J. Mater. Sci.*, 2001, **36**, p 3833–3854

21. H.J. McQueen, S. Spigarelli, M.E. Kassner, and E. Evagelista, *Hot Deformation and Processing of Aluminum Alloys*, CRC, Bradenton, FL, 2011, p 87–190

22. F.J. Humphreys and M. Hatherly, *Recrystallization and Related Annealing Phenomena*, 2nd ed., Elsevier, Oxford, 2004, p 169–213, 415–450

23. H.J. McQueen, Metal Forming: Industrial, Mechanical Computational and Microstructural, *J. Mater. Process. Technol.*, 1993, **37**, p 3–36

24. S. Banerjee, P.S. Robi, A. Srinivasan, and L. Praveen Kumar, High Temperature Deformation Behavior of Al-Cu-Mg Alloys Micro-Alloyed with Sn, *Mater. Sci. Eng. A*, 2010, **527**, p 2498–2503

25. S.B. Brown, K.H. Kim, and L. Anand, An Internal Variable Constitutive Model for Hot Working of Metals, *Int. J. Plast.*, 1989, **5**, p 95–130

26. S. Mandal, V. Rakesh, P.V. Sivaprasad, S. Venugopal, and K.V. Kasiviswanathan, Constitutive Equations to Predict High Temperature Flow Stress in a Ti-Modified Austenitic Stainless Steel, *Mater. Sci. Eng. A*, 2009, **500**, p 114–121

27. Z.Y. Chen, S.Q. Xu, and X.H. Dong, Deformation Behavior of AA6063 Aluminium Alloy After Removing Friction Effect Under Hot Working Conditions, *Acta Metall. Sin.*, 2008, **21**, p 451–458

28. W. Li, H. Li, Z. Wang, and Z. Zheng, Constitutive Equations for High Temperature Flow Stress Prediction of Al-14Cu-7Ce Alloy, *Mater. Sci. Eng. A*, 2011, **528**, p 4098–4103

29. A. Marandi, A. Zarei-Hanzaki, N. Haghdadi, and M. Eskandari, The Prediction of Hot Deformation Behavior in Fe-21Mn-2.5Si-1.5Al Transformation-Twinning Induced Plasticity Steel, *Mater. Sci. Eng. A*, 2012, **554**, p 72–78

30. C.M. Sellar and W.J.M. Tegart, Hot Workability, *Int. Met. Rev.*, 1972, **17**, p 1–24

31. H.J. McQueen and P. Sakaris, Influence of Stress Multiplier in SINH Equation on Constitutive Constants for Al Alloys with Mg and Dispersoids, Aluminum Alloys: Their Physical and Mechanical Properties (ICAA3), L. Arnberg, E. Nes, O. Lohne, and N. Ryum, Ed., June 22-26, 1992 (Trondheim, Norway), The Norwegian Institute of Technology and SINTEF Metallurgy, 1992, vol. 2, p 179–184

32. P. Liu, T. Thorvaldsson, and G.L. Dunlop, Formation of Intermetallic Compounds During Solidification of Dilute Al-Fe-Si Alloys, *Mater. Sci. Technol.*, 1986, **2**, p 1009–1018

33. P. Skjerpe, Intermetallic Phases Formed During DC-Casting of an Al-0.25 Wt Pct Fe-0.13 Wt Pct Si Alloy, *Metall. Trans. A*, 1987, **18**, p 189–200

34. M. Shakiba, N. Parson, and X.-G.Chen, Effect of Homogenization Treatment and Silicon Content on the Microstructure and Hot Workability of Dilute Al-Fe-Si Alloys, *Mater. Sci. Eng. A*, 2014, **619**, p 180–189

35. H.J. McQueen, W.A. Wong, and J.J. Jonas, Deformation of Aluminium at High Temperatures and Strain Rates, *Can. J. Phys.*, 1967, **45**, p 1225–1234

36. J.J. Jonas, D.R. Axelrad, and J.L. Uvira, On Substructure Strengthening and the High Temperature Deformation of Cubic Metals, *Trans. Jpn. Inst. Met.*, 1968, **9**, p 257–267

37. J. Zhang, F. Pan, R. Zuo, and C. Bai, The Low Temperature Precipitation in Commercial-Purity Aluminium Sheets for Foils, *J. Mater. Process. Technol.*, 2008, **206**, p 382–387